LAWRENCE
LIVERMORE
NATIONAL
LABORATORY

LLNL-JRNL-557544

# Energetics and approximate quasiparticle electronic structure of low-index surfaces of SnO2

S. Kuefner, A. Schleife, B. Hoeffling, F. Bechstedt

May 14, 2012

Physical Review B

## Disclaimer

# Energetics and approximate quasiparticle electronic structure of low-index surfaces of $SnO_2$

Sebastian Küfner,[1,2,*] André Schleife,[2,3] Benjamin Höffling,[1,2] and Friedhelm Bechstedt[1,2]

[1]*Institut für Festkörpertheorie und -optik, Friedrich-Schiller-Universität, Max-Wien-Platz 1, 07743 Jena, Germany*
[2]*European Theoretical Spectroscopy Facility (ETSF)*
[3]*Condensed Matter and Materials Division, Lawrence Livermore National Laboratory, Livermore, California 94550, USA*

(Dated: May 8, 2012)

The geometry and energetics of the unreconstructed tin- and oxygen-terminated (100), (010), and (110) surfaces, the tin-terminated (111) surface, and the stoichiometric (001) surface of rutile-$SnO_2$ are investigated. Total energies and relaxed atomic geometries are calculated within density functional theory using the local density approximation (LDA). We conclude from these results that the (110) and (100) surfaces are most stable. Their termination depends on the experimental situation: while under oxygen-rich preparation conditions the oxygen termination is preferred, reduced surfaces are more likely to occur in the oxygen-poor limit. In addition, electronic band structures and densities of states are calculated using a recently developed approximate quasiparticle approach, the LDA-$\frac{1}{2}$ method. All but the SnO-terminated (110) surface are found to be insulating and O- or Sn-derived surface states appear in the projected bulk fundamental gap. While the surface barrier heights vary by more than 2 eV with orientation and termination, we find that the energetically favored surfaces tend to give the lower ionization energies.

PACS numbers: 68.35.bg, 68.35.Md, 73.20.At, 79.60.Bm
Keywords: tin dioxide, surface energies, surface thermodynamics, surface relaxation, band structure, ionization energy

## I. INTRODUCTION

Transparent conducting oxides have attracted much attention due to their exceptional physical properties and a variety of possible applications.[1,2] They form a class of materials that are highly transparent for light in the visible and ultraviolet spectral range and that are highly conductive at the same time. One particularly interesting representative is tin dioxide ($SnO_2$) which has been known for one century as the mineral *cassiterite* or simply as stannic oxide. $SnO_2$ crystallizes in the rutile (*rt*) structure [space group $P4_2/mnm$ or $D_{4h}^{14}$ (SG 136)] under ambient conditions.[3,4] Films of $SnO_2$ are widely used for transparent electrodes in optoelectronics, for instance in solar cells or display devices, but also for gas sensing applications.[5–7] In this context, especially the high efficiency of antimony doping has proven to be beneficial and is known for years.[8–11] In addition to the large fundamental band gap, also the static dielectric constant of $SnO_2$ is large, which renders this material interesting for the next-generation gate oxides for Si-based electronic devices.[12,13]

Despite many years of research, several properties of $SnO_2$ are still being subject of current investigations, for instance, the coexistence of unintentional *n*-doping and the optical transparency[12,14] as well as the non-stoichiometry.[15] Only recently a value for the fundamental gap of $E_g \approx 3.6$ eV, as derived from two-photon absorption measurements,[16] was reconciled[17] with the observation that the optical absorption edge occurs about 0.7 eV higher in energy.

While it is known that tin atoms form a body-centered tetragonal sublattice in $SnO_2$ with six oxygen atoms being coordinated to each Sn atom, the Sn cation allows for a dual valence which facilitates a reversible transformation $Sn^{4+} \leftrightarrow Sn^{2+}$. The Sn atoms in $SnO_2$ are quadrivalent, but also metastable SnO (with divalent Sn atoms) exists in the litharge structure. The possibility of Sn being either $Sn^{4+}$ or $Sn^{2+}$ may cause a variety of surface structures[18] and homologous compounds such as $Sn_2O_3$ or $Sn_3O_4$.[19]

Even though numerous experimental[20–24] as well as first-principles studies[18,21,25–29] have been carried out for surfaces of $SnO_2$, several open questions remain. While the oxygen terminated (110) surface is generally considered to be the most stable one, the energetic order of surfaces with different orientation is still being debated.[18,25] In addition, in experiments also the preparation conditions (e.g. the oxygen partial pressure) play an important role[24] as they influence the surface termination. For instance, at high oxygen partial pressures the $1\times1$ termination of the stoichiometric $SnO_2$(110) surface is preferred over reduced surface phases such as $1\times2$ and $4\times1$.[24] Other surface orientations seem to maintain a $1\times1$ reconstruction also under reducing conditions,[29] hence, we focus on unreconstructed surfaces in this work. While for a systematic total-energy study, the influence of the preparation conditions can be simulated by taking the oxygen chemical potential into account,[18,29] this has only been done in Ref. 29 for the calculation of the surface free energies for different terminations of the low-index (001), (100), (010), and (110) surfaces. Unfortunately, an explanation of the findings in terms of the resulting electronic structure and the arrangement of lone pairs is still missing.

In general, little is known about the electronic structures, especially of the non-stoichiometric surfaces: While photoemission spectroscopy (PES) studies[6,20,23] focus on the (110) surface of $SnO_2$, previous theoretical works[18,26–28] suffer from the significant underestimation of the fundamental gaps (by more than 2 eV) that can be attributed to the use of density functional theory (DFT). In addition, also the surface energy barriers for the emission (ionization energy) or the escape (electron affinity) of electrons are not well understood (see Ref. 30 and references therein). The theoretical description can, in principle, be improved by a quasiparticle (QP) approach that properly accounts for the excitation aspect of PES experiments. However, a full QP description is computa-

tionally very expensive.

In this article, we present a detailed study of the stability and the energetic ordering of the low-index surfaces of *rt*-$SnO_2$ based on DFT calculations of the total energies for the relaxed surface geometries. The LDA-$\frac{1}{2}$ scheme[31] is used to calculate approximate QP energies in order to describe surface bands and electronic states. The theoretical and numerical methods are described in Sec. II. We discuss surface energies and geometries in Sec. IV and the surface band structures are analyzed together with ionization energies and electron affinities in Sec. V. Finally, a brief summary and conclusions are given in Sec. VI.

## II. COMPUTATIONAL METHODS

### A. Ground-state calculations

Total energies are computed by means of the DFT[32] within the local density approximation (LDA).[33] Exchange and correlation (XC) are described using the results of Ceperley and Alder[34] as parameterized by Perdew and Zunger.[35] The calculations are carried out using the Vienna *Ab-initio* Simulation Package (VASP).[36,37] To describe the electron-ion interaction and the wave functions in the core region, we apply the projector-augmented wave method.[38,39] The Sn 4*d*, Sn 5*s*, Sn 5*p* as well as the O 2*s* and O 2*p* electrons are treated as valence electrons in our calculations. Between the cores, the wave functions are expanded into plane waves up to a cutoff energy of 400 eV. In the case of bulk $SnO_2$ the Brillouin zone (BZ) integration is replaced by a sum over $6\times6\times9$ Monkhorst-Pack (MP)[40] points. For the surface calculations we use $6\times6\times1$ MP points for the (001) and the (111) surface and $9\times6\times1$ MP points in all other cases.

In order to determine the equilibrium atomic geometries, we use a conjugate-gradient algorithm to relax the positions of the atoms until the forces are smaller than 5 meV/Å. While the ions in the center layers of the surface slabs are kept fixed at their bulk positions, the outermost two [for surfaces with (100) orientation] or three (all other surfaces) atomic layers on each side of the material slab are relaxed.

### B. Electronic-structure calculations

Modern QP approaches to calculate electronic band structures are based on an iterative solution of the QP equation, using, for instance, Hedin's *GW* approximation for the XC self-energy of the electrons, with *G* describing the single-particle Green's function and *W* the screened Coulomb potential.[41] For computational reasons, the fully self-consistent solution of the QP equation is usually replaced by a perturbative approach that corrects a starting electronic structure (eigenvalues and eigenfunctions) which already resembles the final QP solution.[42,43] In the case of oxide[17,44] as well as nitride semiconductors,[45,46] the solution of a generalized Kohn-Sham equation with a spatially non-local XC potential, e.g. the one derived from the hybrid HSE06 functional[47] (using a range separation parameter $\omega = 0.15$ a.u.[48]), has proven to provide a reliable starting electronic structure for calculating QP energies by means of one step of perturbation theory.

This so-called HSE+$G_0W_0$ scheme[42,43] to calculate QP energies is computationally very demanding and, hence, it is not feasible to apply it to the large surface unit cells described below that contain significantly more atoms than the unit cells in the bulk case. Consequently, for surface supercells an approximate treatment of the QP effects is inevitable.[49] In this work we apply the recently developed LDA-$\frac{1}{2}$ method,[31] which is based on the idea of Slater's transition state.[50,51] The QP self-energy effects are simulated by a hole excitation with an extent that is characterized by a radius parameter called CUT. Following the maximization procedure described in Ref. 31, we obtain CUT=1.0 a.u. (Sn atoms) and 2.25 a.u. (O atoms) for the *pd*-like hole excitation with 50 % O *p* character and 50 % Sn *d* character.

The influence of spin-orbit coupling on the band dispersion was found to be negligible for bulk $SnO_2$[17] as well as for the surfaces studied in this work, hence, all calculations were performed without taking this relativistic effect into account.

### C. Surface modeling

In this work, the relaxed (100), (110), (001), and (111) surfaces are simulated using the repeated slab method (see e.g. Ref. 52) for the bulk-determined, unreconstructed $(1\times1)$, lateral two-dimensional (2D) unit cells. In the notation $(hkl)_{\mathrm{Sn}_n\mathrm{O}_m}$ the $(hkl)$ are the Miller indices of the respective surface; the numbers *n* and *m* are used to describe the ratio $(n/m)$ of Sn and O atoms in the surface unit cell for the different terminations. The atomic geometries and the corresponding slabs are shown in Fig. 3 and discussed in detail in Sec. IV.

Adopting the stoichiometry of the bulk crystal also for the material slab can lead to asymmetric structures where the surfaces on the upper and lower slab differ. For non-stoichiometric surfaces the different surface charge densities cause a dipole potential that is obviously non-physical for real structures. It is possible to correct for this artificial dipole moment by adding a linear electrostatic potential in the calculations,[53] however, the use of non-symmetric slabs has another disadvantage: Since both surfaces of non-symmetric slabs are different, it is impossible to calculate surface energies. For these reasons, we study *symmetric* slabs in this work, similar to other authors.[18] The non-stoichiometry that results for the symmetric slabs for the $(100)_{\mathrm{Sn}}$, the $(110)_{\mathrm{SnO}}$, the further reduced $(110)_{\mathrm{Sn_2O}}$, and the $(111)_{\mathrm{Sn}}$ surfaces is presumed to be negligible due to the large number of atoms in each of the supercells. For these symmetric slabs, no dipole corrections to the electrostatic potential[53] are needed and, in addition, it is possible to calculate also the corresponding surface energies.

In each case we checked that the material slab is thick enough to converge the surface energy $\gamma$ within a range of less than 5 meV/Å$^2$. We checked that our supercells contain a large enough vacuum region by ensuring that the electrostatic

potential shows a flat plateau inside the vacuum. Additionally, we checked that the ionization energy was converged to within a range of less than 5 meV.

### D. Surface classification

Since *rt*-$SnO_2$ is a material with strong ionic bonds the ideal low-index surfaces are governed by the electrostatic energy. Assuming that the bonded Sn and O atoms can be considered as point-charge-like ions, we classify the $SnO_2$ surfaces following the scheme of Tasker:[54,55]

(i) Type-I surfaces involve a sequence of neutral ionic planes; surfaces that are formed by these planes are non-polar.

(ii) Type-II surfaces are characterized by a sequence of charged ionic planes with no electric dipole moment in the slab.

(iii) Type-III surfaces are characterized by a stacking of charged ionic planes, leading to a net dipole in the slab and, therefore, polar surfaces. Since we study only symmetric surfaces in this work, none of them is of type III.

### E. Surface thermodynamics

The stability of the surfaces is characterized by the surface energy $\gamma$, which, in general, depends on the surface preparation conditions. Using the Planck grand canonical potential, which depends on the chemical potentials of tin ($\mu_{\rm Sn}^{\rm SnO_2}$) and oxygen ($\mu_{\rm O}^{\rm SnO_2}$) in bulk $SnO_2$, $\gamma$ can be written for symmetric surfaces as[18,29,52,56]

$$\gamma = \frac{1}{2A}[E_{\rm slab}(N_{\rm Sn},N_{\rm O}) - N_{\rm Sn}\mu_{\rm Sn}^{\rm SnO_2} - N_{\rm O}\mu_{\rm O}^{\rm SnO_2}]. \quad (1)$$

Here, $A$ is the surface area of one surface of the slab. The total energy of the slab, $E_{\rm slab}(N_{\rm Sn},N_{\rm O})$, is approximated by the DFT total energy, and $N_{\rm Sn}$ ($N_{\rm O}$) describes the number of tin (oxygen) atoms[52] in the unit cell. We investigate surfaces that are in equilibrium with the underlying bulk substrate, therefore, the chemical potentials of the two elements are related to each other by the chemical potential (per formula unit) of the $SnO_2$ bulk material, $\mu_{\rm SnO_2}^{\rm bulk}$, via

$$\mu_{\rm Sn}^{\rm SnO_2} + 2\mu_{\rm O}^{\rm SnO_2} = \mu_{\rm SnO_2}^{\rm bulk}. \quad (2)$$

In this work we want to study the surface energies as a function of the oxygen chemical potential. In this case, inserting Eq. (2) into Eq. (1) yields

$$\gamma = \frac{1}{2A}[E_{\rm slab}(N_{\rm Sn},N_{\rm O}) - N_{\rm Sn}\mu_{\rm SnO_2}^{\rm bulk} + (2N_{\rm Sn} - N_{\rm O})\mu_{\rm O}^{\rm SnO_2}]. \quad (3)$$

For stoichiometric slabs of $SnO_2$, it holds $N_{\rm Sn} + N_{\rm O} = 3N_{\rm Sn}$ and Eq. (3) reduces to

$$\gamma = \frac{1}{2A}\left[E_{\rm slab}(N_{\rm Sn},N_{\rm O}) - N_{\rm Sn}\mu_{\rm SnO_2}^{\rm bulk}\right]. \quad (4)$$

The pressure dependence of the chemical potential is negligible for solids and, in addition, we assume that also the temperature dependence of the small lattice-vibration contribution is negligible. In this case, we can identify $\mu_{\rm SnO_2}^{\rm bulk}$ with the total energy $E_{\rm bulk}^{\rm SnO_2}$ (per formula unit) calculated within DFT. The range of the oxygen chemical potential is determined by the heat of formation $\Delta H_{\rm f}^{\rm SnO_2}$ of bulk $SnO_2$ which is defined as the energy gain related to the formation of $SnO_2$ from bulk elemental Sn and molecular oxygen, i.e.,

$$\Delta H_{\rm f}^{\rm SnO_2} = \mu_{\rm Sn}^{\rm el} + \mu_{\rm O_2}^{\rm mol} - \mu_{\rm SnO_2}^{\rm bulk}. \quad (5)$$

Setting the energy zero to $\frac{1}{2}E_{\rm O_2}^{\rm mol}$, the oxygen chemical potential varies in the range

$$-\frac{1}{2}\Delta H_{\rm f}^{\rm SnO_2} \le \mu_{\rm O}^{\rm SnO_2} - \frac{1}{2}E_{\rm O_2}^{\rm mol} \le 0. \quad (6)$$

The lower bound describes oxygen-poor conditions (i.e. Sn-rich conditions with $\mu_{\rm Sn}^{\rm el} = \mu_{\rm Sn}^{\rm SnO_2}$), while the upper bound refers to oxygen-rich conditions.

In this work, we computed total energies of $E_{\rm bulk}^{\alpha\text{-Sn}} = -4.24$ eV ($\alpha$-Sn; diamond structure with $a = 4.489$ Å[57]) and $E_{\rm bulk}^{\beta\text{-Sn}} = -3.71$ eV ($\beta$-Sn; space group $I4_1$/amd with $a = 5.832$ Å[57] and $c = 3.181$ Å[57]) for the two bulk phases of Sn. We computed these values within DFT-LDA using a $12\times12\times12$ **k**-point mesh, a plane-wave cutoff of 450 eV, and spin-orbit coupling was taken into account.[58]

For the total energy of the oxygen molecule we computed $E_{\rm O_2}^{\rm mol} = -10.546$ eV, using a supercell with an edge length of 15 Å. Using these values and the total energy of $SnO_2$ (see Sec. III), we find a heat of formation of $\Delta H_{\rm f}^{\rm SnO_2} = 6.32$ eV ($\alpha$-Sn) or 6.85 eV ($\beta$-Sn). These values are similar to other results of 6.342 eV [computed[18] using DFT and the generalized-gradient approximation (GGA)], 6.77 eV (LDA[29]), and 5.5 eV (GGA[29]). The experimental value is about 5.6 eV[59] or 5.98 eV.[60]

The cohesive energy is defined as the energy difference between the bulk substrate and the total energies of the atoms in their respective spin-polarized ground state. We calculated the atomic energies to be $E_{\rm Sn} = -0.375$ eV and $E_{\rm O} = -1.489$ eV, hence, the cohesive energy of bulk $SnO_2$ is given by $E_{\rm coh}^{\rm SnO_2} = E_{\rm Sn} + 2E_{\rm O} - E_{\rm bulk}^{\alpha\text{-Sn}} = 17.75$ eV. The cohesive energy of bulk Sn amounts to $E_{\rm coh}^{\alpha\text{-Sn}} = 4.11$ eV and $E_{\rm coh}^{\beta\text{-Sn}} = 3.33$ eV, which is close to an experimental value of 3.14 eV.[61] Also the binding energy of an $O_2$ molecule calculated in this work, $E_{\rm bind}^{\rm O_2} = 5.32$ eV, is close to the result from experiment of 5.2 eV.[61]

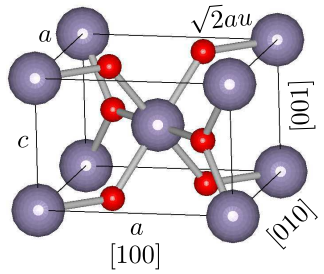


FIG. 1. (Color online) Unit cell and atomic positions of bulk *rt*-$SnO_2$. Grey (large) circles indicate tin atoms, while oxygen atoms are shown as red (small) circles.

## III. BULK TIN DIOXIDE

### A. Structure and energetics

In the bulk *rt* unit cell (cf. Fig. 1), each tin atom is coordinated to six oxygen atoms and each oxygen atom to three tin ions. Tin ions are located at (0, 0, 0) and (0.5, 0.5, 0.5) and the coordinates of the oxygen atoms are $\pm(u, u, 0)$ and $(0.5\pm u, 0.5\mp u, 0.5)$ in units of the crystal axes.[18]

The total energy, the lattice parameters $a$ and $c$, and the bulk modulus $B_0$ (as well as its pressure derivative $B_0'$) are obtained by fitting the dependence of the total energy on the volume to the Murnaghan equation of state.[64] The resulting optimized structural and elastic parameters (see Table I) exhibit minor variations with respect to similar calculations[17] due to the slightly modified cutoff energy and **k**-point sampling. The comparison to a DFT-GGA calculation[18] shows the well-known tendency of underbinding of the GGA with respect to the LDA:[65] The lattice parameter $a$ ($c$) calculated in this work is approximately 0.1 Å (0.4 Å) smaller than the result obtained using the GGA.[18] Even though the comparison with measured values[3,6,57,62,63] indicates excellent agreement for $a$, $u$, and $B_0$, the small overestimation of $c$ by about 0.5 % within DFT-LDA is surprising.

As can be seen from Table I, the total energy of bulk $SnO_2$ calculated in this work is lower than a GGA result[18] and we obtain also a larger cohesive energy. This agrees with the well-known tendency of the LDA to overbind.[66]

### B. Electronic structure

In the following, we compare HSE+$G_0W_0$ results[17] for the band structure and the density of states (DOS), that have been successfully used to explain the electronic structure of *rt*-$SnO_2$, to the LDA-$\frac{1}{2}$ results for the bulk material (see Fig. 2). The states that form the fundamental gap have the same atomic origin in both cases: while the uppermost valence bands are mainly of O 2*p* type, the lowest conduction bands show a strong Sn 5*s* and Sn 5*p* character. Figure 2 also shows that the fundamental gap calculated within the LDA-$\frac{1}{2}$ scheme, $E_g = 3.30$ eV, is about 0.3 eV lower compared to the

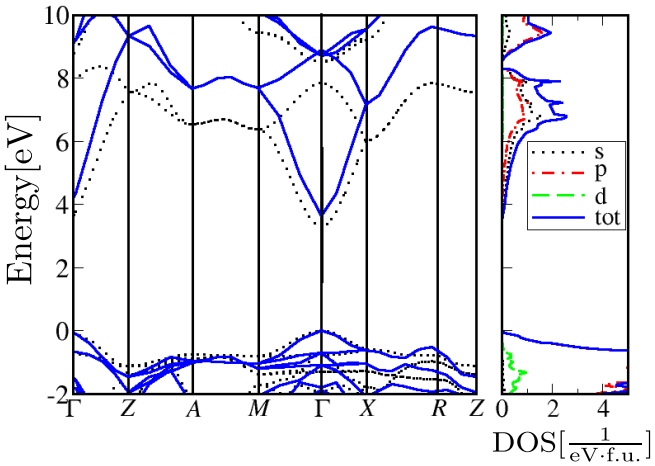


FIG. 2. (Color online) The QP band structure of *rt*-$SnO_2$ as calculated within the LDA-$\frac{1}{2}$ scheme (dotted lines) is compared to the HSE+$G_0W_0$ results (solid lines) of Ref. 17. The valence-band maximum is used as energy zero. In addition, the angular-momentum-resolved DOS, calculated using the LDA-$\frac{1}{2}$ scheme, is given in order to describe the atomic origin of the respective states.

QP calculation ($E_g = 3.61$ eV).[17] Hence, the difference to the experimental value of 3.56 eV[67] amounts to 250 meV. This deviation is a remarkable improvement over the DFT-LDA result that is as small as $E_g = 1.03$ eV, a value that DFT-GGA ($E_g = 0.69$ eV[18]) does not improve on.

Also with regard to the band width and dispersion of the uppermost valence bands the HSE+$G_0W_0$ and the LDA-$\frac{1}{2}$ approximations agree well: The deviation of the QP energy of the highest valence bands is 0.32 eV at the $Z$ point of the BZ and the deviation of the highest valence bands in the energy range between $-2$ and 0 eV is smaller than 200 meV. In addition, the band width of the uppermost valence band complex is 7.3 eV (LDA-$\frac{1}{2}$) or 8.3 eV (HSE+$G_0W_0$), whereas the ultraviolet photo-electron spectroscopy gives about 9 eV.[9,10] The position of the Sn 4*d* and O 2*s* states (not shown in Fig. 2) was found to be around 2 eV too high in LDA-$\frac{1}{2}$. However, since we are interested in surface states inside the fundamental gap of the bulk, the deviations of the LDA-$\frac{1}{2}$ results at energies even lower than $-2$ eV below the valence-band maximum (VBM) are not expected to strongly influence the surface states in the bulk fundamental gap. We find that the lowest LDA-$\frac{1}{2}$ conduction bands are 0.3 eV below the HSE+$G_0W_0$ QP bands at Γ, but about 1.3 eV lower at the BZ boundary.

Overall, the LDA-$\frac{1}{2}$ approach yields satisfying results at much lower computational cost (with respect to HSE+$G_0W_0$), even though the agreement with the QP scheme is not perfect. Since the valence band width is only slightly more underestimated[68] and the band gaps are in reasonable agreement, we use this method to investigate electronic properties of surfaces in this work.

TABLE I. The lattice constants $a$ and $c$ (in Å), the dimensionless parameters $c/a$ and $u$, the bulk modulus $B_0$ (in GPa) and its pressure derivative $B_0'$, as well as the total energy $E_{\rm bulk}^{\rm SnO_2}$ and the cohesive energy $E_{\rm coh}$ (in eV) per formula unit are compared to a DFT-GGA work and experiment.

| | $a$ (Å) | $c$ (Å) | $c/a$ | $u$ | $B_0$ (GPa) | $B_0'$ | $E_{\rm bulk}^{\rm SnO_2}$ (eV) | $E_{\rm coh}$ (eV) |
|---|---|---|---|---|---|---|---|---|
| This work (LDA) | 4.732 | 3.201 | 0.6764 | 0.306 | 215 | 4.7 | −21.106 | 17.75 |
| Expt. | 4.74[a,c,d,e,f] | 3.19[a,c,d,e,f] | 0.673[a,c,d,e,f] | 0.307[a,d] | 205[a] | 7.4[a] | - | 15.5[b] |
| Theory (GGA) | 4.821[g] | 3.236[g] | 0.6712[g] | - | 179[g] | 5.0[g] | −18.938[g] | 16.07[g] |

[a] Ref. 3
[b] Value cited in Ref. 18
[c] Ref. 62
[d] Ref. 63
[e] Ref. 57
[f] Ref. 6
[g] Ref. 18

TABLE II. Displacements (in Å) of atoms (calculated as the difference between the Cartesian coordinates of the relaxed ionic positions and the ideal ones) in the different layers of the relaxed surfaces. Due to the symmetry of the slabs the displacements of the atoms are only given for the upper surface (for the other side, these values are equal, but the sign is reversed). For the $z$ coordinate, a positive sign refers to a displacement of the atom in the direction of the vacuum.

| Surface | First layer | Second layer | Third layer |
|---|---|---|---|
| $(001)_{\rm SnO_2}$ | Sn (0.01, 0.01, 0.10) | Sn (0.00, 0.00, 0.40) | Sn (0.01, 0.01, 0.17) |
| | O (-0.09, 0.10, 0.42) | O (-0.02, -0.02, 0.20) | O (-0.02, 0.03, 0.28) |
| | O (0.10, 0.09, 0.42) | O (0.04, 0.04, 0.20) | O (0.03, -0.02, 0.28) |
| $(100)_{\rm O}$ | O (0.28, 0.30, 0.19) | Sn (0.06, 0.00, 0.04) | |
| $(100)_{\rm Sn}$ | Sn (0.16, 0.00, 0.18) | O (0.02, 0.00, 0.17) | |
| $(110)_{\rm O}$ | O (0.00, 0.00, 0.05) | Sn (0.02, 0.00, 0.17) | |
| | | Sn (0.00, -0.35, 0.17) | |
| | | O (0.02, -0.07, 0.18) | |
| | | O (0.02, 0.02, 0.17) | |
| $(110)_{\rm SnO}$ | O (0.01, -0.04, 0.19) | O (0.00, -0.03,-0.03) | O (0.0, 0.0, -0.06) |
| | Sn (0.00, 0.00, -0.12) | | |
| | O (0.01, -0.02, 0.19) | | |
| | Sn (0.01, -0.03, 0.05) | | |
| $(110)_{\rm Sn_2O}$ | O (0.03, 0.06, 0.11) | O (0.00, 0.00,0.02) | |
| | Sn (0.00, 0.11, 0.01) | | |
| | Sn (0.03, 0.02, 0.03) | | |
| $(111)_{\rm Sn}$ | Sn (-0.03, 0.02, 0.16) | O (0.00,-0.02, 0.12) | O (0.01, -0.05, 0.18) |
| | | | O (0.03,-0.04, 0.18) |
| | | | Sn (-0.08, 0.09, -0.02) |

## IV. SURFACES OF $SnO_2$: STRUCTURE AND ENERGETICS

### A. Structural relaxation

As explained in Sec. I, tin has two stable ions, $Sn^{2+}$ and $Sn^{4+}$. In bulk $SnO_2$, Sn is four times positively charged. Due to the removal of oxygen atoms in order to form a surface, this number is changed. Hence, there is a tendency either to regain the $Sn^{4+}$ state, or, in most cases, to form $Sn^{2+}$ ions in the surface region. This can be achieved by the transfer of electrons from the tin dangling bonds into an oxygen $2p$ orbital near the surface. However, this might be a driving force for the displacement of the atoms near the surface and in the following this will be investigated for the different surfaces.

#### 1. (001) surface

The non-polar and stoichiometric (001) surface is a type-I surface and we describe it using an 11-layer $Sn_{11}O_{22}$ slab. Each surface unit cell (area $A = a^2 = 22.39$ Å$^2$) consists of one formula unit of $SnO_2$, hence, we denote this surface as $SnO_2$-terminated. The two oxygen atoms in each $(1\times1)$ cell are twofold coordinated, in contrast to the bulk situation. The coordination of the Sn atom in the first atomic layer is reduced to four: there are two bonds to oxygen atoms in the same plane and two bonds to O atoms in the plane underneath [see Fig. 3(b) and (c)].

The atoms in the uppermost surface layers relax towards the outside of the material, starting from their bulk positions. Due to the different displacements of Sn and O atoms in normal direction, all the layers are buckled. In addition to this vertical displacement, the oxygen atoms are also shifted perpendicular to the surface normal (cf. Table II). As a consequence of these relaxations, the Sn-O bond lengths are reduced by 0.14 Å and the second-nearest-neighbor O-O distances increase by 0.13 Å at the surface. These effects are explained by the opposite ion charges of the one tin ($Sn^{4+}$) and two oxygen ($O^{2-}$) atoms in the unit cell of the uppermost surface layer and the corresponding Coulomb attraction or repulsion. The relaxation of the surface reduces the surface energy $\gamma$ by 35 meV/Å$^2$.

#### 2. (100) surfaces

The non-stoichiometric type-I Sn- and O-terminated (100) surfaces (cf. Fig. 3) are symmetry-equivalent to the (010) surfaces (cf. Fig. 1) and the distance of two adjacent Sn layers amounts to $a/2$. The oxygen layers in between have a distance of $a(0.5-u)$ and $ua$ to the Sn layer above and underneath, respectively. The $(1\times1)$ unit cell contains one atom in each layer and the symmetric irreducible part of the material

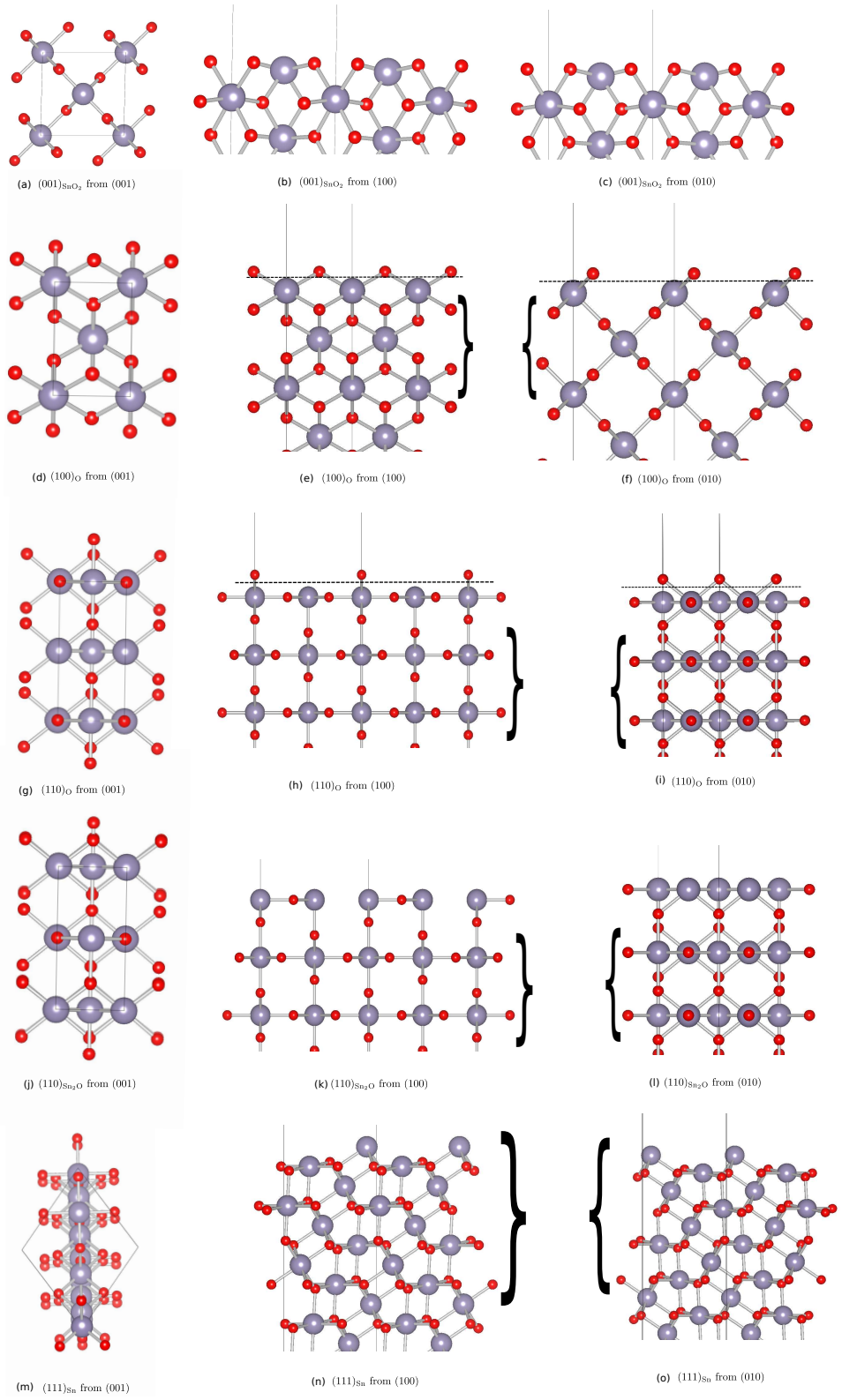


FIG. 3. (Color online) Unrelaxed atomic geometries of the surfaces studied in this work: (a)−(c) $(001)_{SnO_2}$, (d)−(f) $(100)_O$, (g)−(i) $(110)_O$, (j)−(l) $(110)_{Sn_2O}$, and (m)−(o) $(111)_{Sn}$. For each orientation, the projections on the three directions (001), (100), and (010) (in direct coordinates of the supercell) are shown. The 2D $(1\times1)$ surface unit cells and the entire slabs are indicated by thin solid lines. Blue (large) circles indicate tin atoms, while oxygen atoms are shown as red (small) circles. The dashed lines indicate which layers have to be removed in order to form the reduced surfaces. The brackets mark the symmetry-irreducible parts of the slabs.

slab in the direction of the surface normal consists of six layers: Sn-O-O-Sn-O-O [cf. Fig. 3(e) and (f)].

In the case of the $(100)_O$ surface one bond at an O atom and one at a Sn atom are broken in the first two layers, hence, the oxygen atom in the first layer is twofold coordinated and the Sn atoms in the second layer are fivefold coordinated. We use a $Sn_9O_{18}$ slab consisting of four irreducible parts Sn-O-O-Sn-O-O and one additional oxygen layer at the bottom as well as one additional Sn-O layer at the top in order to obtain a symmetric slab.

When the topmost and lowest oxygen layers are removed, the resulting $(100)_{Sn}$ surface becomes tin-terminated. While in this case all oxygen atoms possess the same coordination as in the bulk, the first-layer tin atoms are threefold coordinated. As a consequence only $Sn^{2+}$ ions occur in the uppermost layer. We use a non-stoichiometric $Sn_9O_{16}$ slab that contains 25 atomic layers to model this surface.

Apart from small lateral atomic displacements, the outermost two atomic layers move outward from the material slab during the relaxation (cf. Table II). Our results are in qualitative agreement with those of Duan,[18] who only investigated the oxygen-terminated surface.

### 3. (110) surfaces

Even when restricting to unreconstructed surfaces and $(1\times1)$ unit cells (area $A = ac/2$), a variety of different (110) surfaces exists depending on termination and oxygen content. Two of the most stable ones[6,18,20,28,29] are depicted in Fig. 3. A bulk-derived slab in this direction consists of neutral groups of six parallel planes O-$Sn_2O_2$-O-O-$Sn_2O_2$-O [see e.g. Fig.3(h) and (i)].

The cleavage cut between these groups of planes breaks the smallest number of cation-anion bonds and leads to the stoichiometric $(110)_O$ surface. Despite the oxygen termination [see Fig. 3(h)], the total dipole moment of the triple layer in the $(1\times1)$ cell vanishes, therefore, this surface is of type II. We model it by using an orthorhombic $Sn_{10}O_{20}$ slab with five triple layers, i.e., 15 atomic layers. The first oxygen layer consists of rows of singly coordinated 'bridging' O atoms in [001] direction [cf. Fig. 3(h) and (i)]. The tin atoms of the second atomic layer are inequivalent since they are either sixfold or fourfold coordinated. Together with the two dangling bonds of the first-layer O atoms, four dangling bonds appear with a total of four valence electrons. The two Sn atoms have no chance to form $Sn^{4+}$ or $Sn^{2+}$ ions in the unrelaxed surface. Therefore, significant atomic displacements are observed for the second $(SnO)_2$ layer to modify the coordination, while the oxygen atoms in the first layer are influenced less (see Table II). The most remarkable effect is a vertical shift of the entire $(SnO)_2$ layer towards the vacuum, nearly leading to a $Sn_2O_3$ layer. In addition, we observe a lateral shift of one Sn atom parallel to the [010] direction. Overall, the atomic relaxations lead to more or less sixfold coordinated Sn atoms and two threefold and one twofold coordinated O atom. These results agree well with the displacements calculated by Duan *et al.*[18] within DFT-GGA; the values differ by less than 0.01 Å. However, the values calculated by Mäki-Jaskari and Rantala are higher by approximately 25 %. This might be an effect of a different number of non-valence electrons for the tin atoms and a different type of pseudopotentials.[28]

Removing the uppermost rows of oxygen atoms leads to the $(110)_{SnO}$ surface with an outermost plane consisting of two tin and two oxygen atoms. The existence of this reduced surface is strongly supported by early Auger measurements[69,70] and its atomic geometry has been previously proposed by other authors.[71] We use four additional triple layers [with respect to the $Sn_{10}O_{20}$ slab discussed for the $(110)_O$ surface above], i.e., a $Sn_{18}O_{34}$ slab, to improve the accuracy of our surface modeling. In the surface unit cell, there are one fivefold and one fourfold coordinated Sn atom and two oxygen atoms that exhibit a bulk-like threefold coordination. Hence, three Sn dangling bonds occur with a total number of two electrons which may form a lone pair in one of these dangling bonds. The Sn atoms in the plane show different displacements due to their different original coordination. While the fivefold coordinated Sn atom and the two oxygen ions of the first layer are shifted outwards, the fourfold coordinated Sn atom is moved towards the bulk. The oxygen ions of the second and third layer are also moved inwards. However, similarly to the (stoichiometric) $(110)_O$ surface, the outward relaxation given in Table II is smaller than those calculated by other authors but using similar methods.[26–28] Unfortunately, Duan[18] did not discuss this surface.

When the high-density $(SnO)_2$ plane is also removed, an oxygen-terminated surface with two uppermost O layers remains (not shown in Fig. 3). In our total-energy calculations this surface turned out to be rather unstable, hence, we will not further discuss it.

Bergermayer and Tanaka[72] have recently suggested a further stabilization of the $(110)_{SnO}$ surface due to removal of every second in-plane oxygen atom [cf. Fig. 3(j), (k) and (l)]. In this case, a trigonal-pyramidal arrangement of Sn with the chance for a lone-pair localization occurs. The corresponding surface unit cell contains two threefold coordinated Sn and one threefold coordinated O atom. However, there are only minor displacements due to the ionic relaxation: the tin atom remaining in the topmost atomic layer is shifted in lateral direction such that the distance between one tin atom and the remaining oxygen atom is increased by 0.11 Å. Furthermore, similar to the $(110)_{SnO}$ surface, the oxygen atom from the second atomic layer is shifted up towards the first atomic layer.

### 4. (111) surfaces

Because of the differences of the *c* and *a* axes of the rutile structure, the (111) surfaces have a more complex atomic geometry. The bulk-derived 2D Bravais lattice is oblique and the $(1\times1)$ unit cell represents a strongly distorted hexagon with an angle of about 108°. In model calculations this surface has been found to be the second most unstable.[73] Here, we focus on the Sn termination, i.e., the topmost layer is formed by

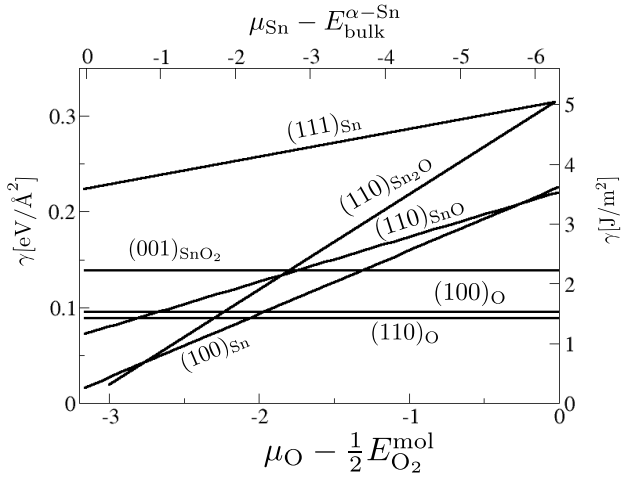


FIG. 4. (Color online) The surface energy $\gamma$ (in eV on the left axis and in J/m$^2$ on the right axis) of the low-index surfaces of $SnO_2$ is given as a function of the O and Sn chemical potential. The O chemical potential is given with respect to the binding energy of the oxygen molecule and the Sn chemical potential with respect to the total energy (per atom) of $\alpha$-Sn. For the $\beta$-Sn phase the axis has to be shifted by 0.71 eV towards higher chemical potentials $\mu_{\rm Sn}$.

rows of Sn ions. They are separated by a horizontal distance of 5.4 Å [see Fig. 3(m), (n), and (o)]. In-between these rows of Sn atoms lower layers of O appear which are bonded to the topmost surface atoms. The tin ions of the surface exhibit three dangling bonds due to a reduction of the coordination number. The oxygen atoms in the second layer are twofold coordinated. However, the vertical distance between the second and the third atomic layer is only 0.2 Å. The tin ions of the third atomic layer are fivefold coordinated and the corresponding oxygen atoms twofold. In total there are four Sn and one O dangling bonds in the surface unit cell. These dangling bonds generate four electrons which can lead to two bonds or lone pairs.

In this work we study a $Sn_{17}O_{32}$ slab. All atoms of the first three layers relax towards the vacuum, while the Sn ion of the third row remains quite unchanged. For all atoms, the displacements perpendicular to the surface normal are smaller than 0.1 Å. The displacements in direction of the surface normal (cf. Table II) are in qualitative agreement with those derived by Duan.[18]

### B. Surface stability

To study the relative stability of the surfaces with different orientation and termination we plot the surface energy, Eq. (3), versus the chemical potential of oxygen, $\mu_{\rm O}^{\rm SnO_2}$, in Fig. 4. From this figure it becomes clear that in a wide range of preparation conditions the stoichiometric, oxygen-terminated $(110)_{\rm O}$ and $(100)_{\rm O}$ surfaces are the most stable ones. The energy difference between these two is small, however, the $(110)_{\rm O}$ surface can be identified as the cleavage face of *rt*-$SnO_2$, and the stoichiometric $(001)_{\rm SnO_2}$ surface is much higher in energy (cf. Fig. 4).

TABLE III. The surface energies $\gamma$ (in J/m$^2$) of three stoichiometric low-index $SnO_2$ surfaces as calculated using different XC functionals (LDA, GGA, and B3LYP) or model potentials are compared. The values of Ref. [29] are derived from Fig. 1 in that paper.

| Surface | This work | LDA | GGA | B3LYP | ionic potentials |
|---|---|---|---|---|---|
| $(110)_{\rm O}$ | 1.435 | 1.44[a] | 1.035[b], 1.3[c], 1.04[e] | 1.20[f] | 1.380[g] |
| $(100)_{\rm O}$ | 1.568 | 1.60[a] | 1.128[b], 1.14[e] | 1.27[f] | 1.664[g] |
| $(001)_{\rm SnO_2}$ | 2.25 | 2.24[a] | 1.72[d], 1.84[e] | 1.84[f] | 2.366[g] |

[a] Ref. [29] [b] Ref. [18] [c] Ref. [28] [d] Ref. [74]
[e] Ref. [75] [f] Ref. [25] [g] Ref. [73]

Under O-poor or Sn-rich preparation conditions for which $\mu_{\rm O} - \frac{1}{2}E_{\rm O_2}^{\rm mol} < -2.0$ eV [$\mu_{\rm O} - \frac{1}{2}E_{\rm O_2}^{\rm mol} < -2.7$ eV], the reduced $(100)_{\rm Sn}$ [$(110)_{\rm Sn_2O}$] surface becomes more favorable. The $(111)_{\rm Sn}$ surface is found to be the most unstable one in the entire range of preparation conditions. The phase diagram in Fig. 4 is in qualitative agreement with that of Ágoston and Albe.[29] The fact that under oxygen-rich conditions the oxygen-terminated $(110)_{\rm O}$ and $(100)_{\rm O}$ surfaces are the most stable ones is in accordance with experimental findings[6,20] and other calculations.[18]

A comparison of the surface energies calculated in this work to results of other calculations is given in Table III for the stoichiometric surfaces. The sequence of the energies is independent of the approximation used. The agreement with another calculation using LDA[29] is excellent as the results differ by less than 0.1 eV/Å. Within the GGA the resulting energies are somewhat smaller.[18,28,74,75] Surprisingly, also the results obtained by total energy calculations based on empirical ionic potentials[73] are rather similar to those from the LDA. The non-local XC functional B3LYP gives rise to surface energy values in-between those from LDA and GGA.[25]

## V. SURFACES OF $SnO_2$: ELECTRONIC STRUCTURE

In the previous section we described that there is a tendency to form $Sn^{2+}$ or $Sn^{4+}$ ions in the vicinity of the surface by transferring electrons from tin dangling bonds into $2p$ states of oxygen atoms near the surface. In the following, we will show that these filled O $2p$ orbitals form surface states inside the fundamental band gap resulting in an insulating behavior of the surface.

### A. (001) surface

The band structure and the DOS of the $(001)_{\rm SnO_2}$ surface is displayed in Fig. 5. All the electronic states in this symmetric slab are are twofold degenerate; the splittings due to residual quantum confinement in the material slab at the $\Gamma$ point are smaller than 0.1 eV.

Figure 5(a) clearly shows pronounced surface bands in the

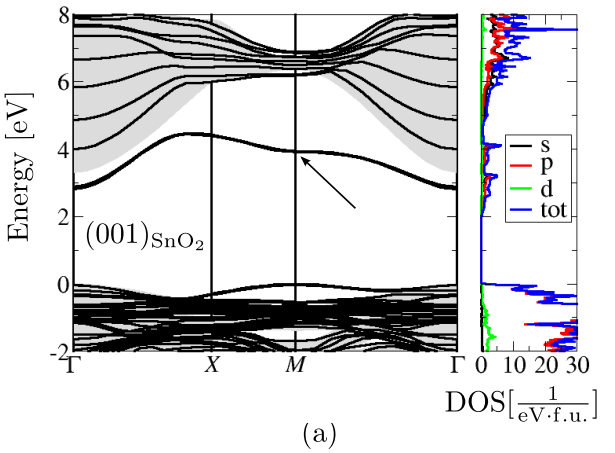


(a)

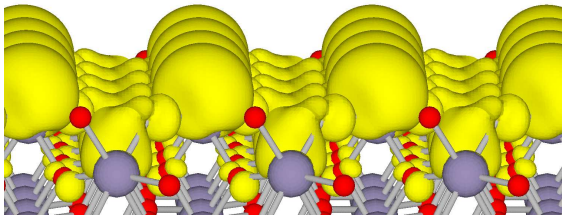

(b)

FIG. 5. (Color online) In (a) the band structure and DOS of the $(001)_{SnO_2}$ surface, calculated using the LDA-$\frac{1}{2}$ scheme, is compared to the projected bulk bands (shaded area). The Fermi level is indicated as blue dashed line. The energy scales of slab and bulk band structures are aligned via the electrostatic potentials.[76] This procedure allows to use the bulk VBM as energy zero. In (b) the square of the wave-function of the empty surface band state at $M$ [the corresponding state is marked by the arrow in (a)] in the fundamental gap is plotted. The yellow isosurfaces represent same probabilities.

projected fundamental bulk gap: Besides the two oxygen-derived occupied bands in the lower part of the fundamental gap near the $M$ point, there is an empty surface band with rather strong dispersion which is mainly composed of Sn 5$s$ states [see Fig. 5(b)]. In order to visualize the orbital and symmetry character of these, the square of the wave function of the empty surface band states at the surface BZ corner $M$ is plotted in Fig. 5(b).

Since all surface bands are either fully occupied or empty, the surface is insulating and this indicates that there should be no driving forces for surface reconstruction. However, the existence of oxygen-derived occupied surface bands indicates the transfer of electrons from the tin dangling bonds into the oxygen 2$p$ orbitals as explained in Sec. IV A.

### B. (100) surfaces

Also in the case of the stoichiometric oxygen-terminated $(100)_O$ surface two occupied surface bands appear, as can be seen from Fig. 6(a). They are located at about 0.2 eV above the bulk VBM along the $X-M$ line. In addition, Fig. 6(c) confirms that charge is transferred from the Sn dangling bond into one O dangling bond and, hence, this leads to a lone pair at each first-layer oxygen atom. This uppermost surface state is formed by in-plane O 2$p$ orbitals in the first atomic layer and O 2$p$ orbitals in the third layer. Surprisingly, the fivefold coordinated Sn ions in the second atomic layer do not contribute to bound surface states. The occurrence of these occupied surface states confirms earlier calculations[18] and there are also experimental indications for such a surface state.[21]

In the case of the reduced, non-stoichiometric Sn-terminated $(100)_{Sn}$ surface the band structure is completely different [cf. Fig. 6(b)]. There are two types of surface band states in the fundamental bulk band gap: (i) an occupied band with strong dispersion (band width: about 1.5 eV), and (ii) an empty band of resonant surface states along the BZ boundary. The DOS of the occupied band exhibits a significant constant contribution which is related to the nearly parabolic parts of the surface bands in the projected gap. Its van Hove singularity near Γ leads to a peak almost 1 eV above the VBM. The DOS indicates that the occupied surface band is built by Sn 5$s$ and O 2$p$ states. Figure 6(d) indicates that these states are localized in the first Sn and second O layer.

### C. (110) surfaces

The band structures and DOS of the O-, SnO- and $Sn_2O$-terminated (110) surfaces are displayed in Figs. 7(a), 7(c) and 7(e). In the case of the oxygen-terminated $(110)_O$ surface there are similarities with the band structure of $(100)_O$ [cf. Fig. 6(a)]. Surface-state bands only appear close to the bulk band edges and indicate an insulating surface with a surface gap of about 1.8 eV near Γ. The uppermost occupied surface band is mainly built by in-plane O 2$p$ orbitals localized at the bridging O atoms in the first atomic layer, as clearly demonstrated in Fig. 7(b). These states result, like in the case of the $(100)_O$ surface, from dangling bonds of the topmost oxygen layer.

The surface band close to the projected bulk band structure is mainly composed of Sn 5$s$ and Sn 5$p$ states. The existence of these surface states was also reported by Duan,[18] Mäki-Jaskari,[28] and Rantala,[27] based on DFT-GGA calculations. By means of PES, Cox[10] and Themlin[23] measured this Sn 5$s$ and Sn 5$p$ derived surface-band whose states are located at the $Sn^{2+}$ ions.

The $(110)_{SnO}$ surface exhibits an extremely dispersive surface band in the projected fundamental gap [cf. Fig. 7(c)] which is crossed by the Fermi level near the $M$ point of the BZ. For that reason, a few bulk-like conduction-band states in the slab center are occupied with electrons. However, it is not clear, whether this effect is real or merely a consequence of the LDA-$\frac{1}{2}$ approximation to XC. This dispersive

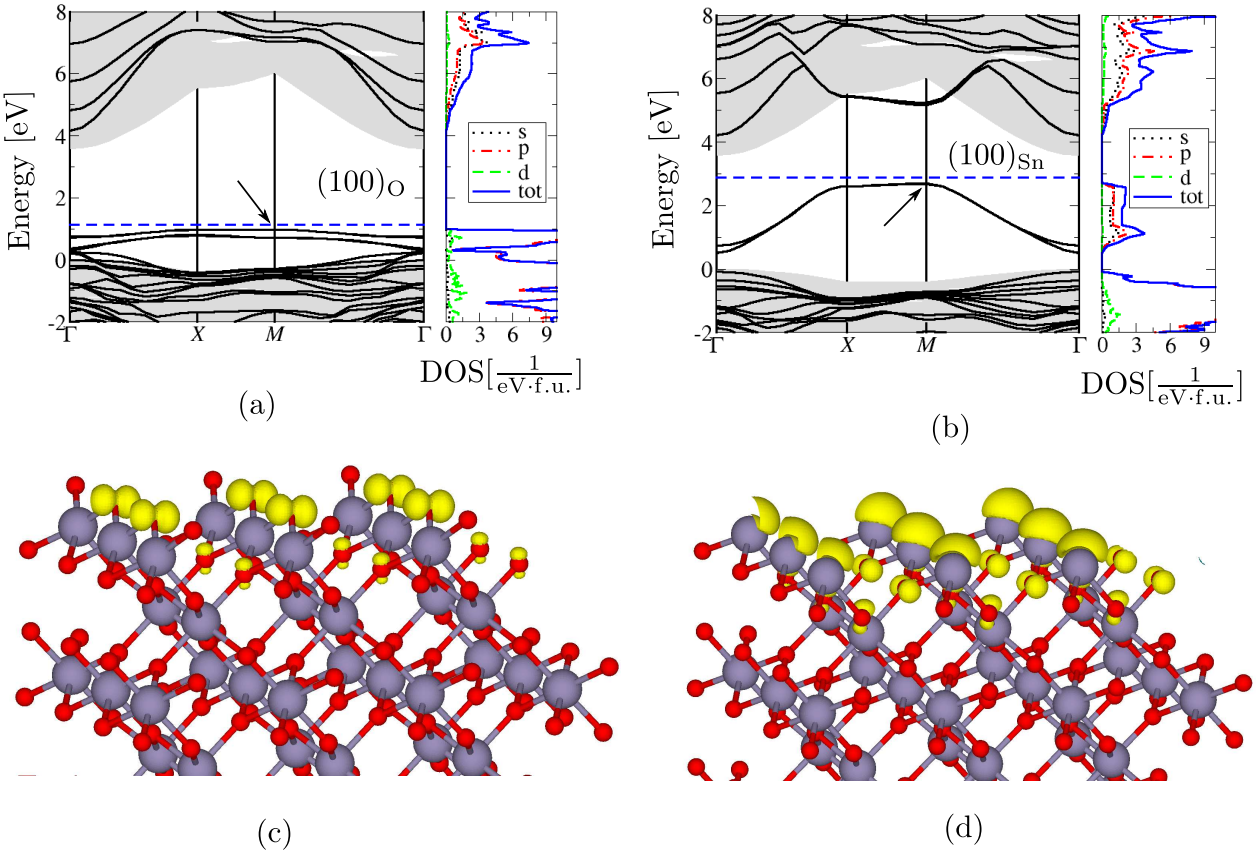


FIG. 6. (Color online) The band structure and DOS of the $(100)_{\mathrm{O}}$ surface (a) and the $(100)_{\mathrm{Sn}}$ surface (b), calculated using the LDA-$\frac{1}{2}$ scheme, is compared to the projected bulk bands (shaded area), respectively. In (c) and (d) the squares of the wave-functions of the highest occupied surface band states at $M$ in the fundamental gap are plotted [the corresponding state is marked by the arrow in (a)]. The yellow isosurfaces represent same probabilities.

band is mainly formed of both Sn (mainly in the first layer) and O states (mainly in the second atomic layer). The resulting band structures for the $(110)_{\mathrm{SnO}}$ surface in Fig. 7(c) is in qualitative agreement with pseudopotential calculations,[27,28] although they are influenced by the DFT gap underestimation.

The electronic structure of the $(110)_{\mathrm{Sn_2O}}$ surface [cf. Fig. 7(e)] shows two rather dispersive surface states in the fundamental bulk band gap that are formed of Sn 5$s$ and Sn 5$p$ states as well as some small contributions from the O 2$p$ states from the O ions in the first and second atomic layer. The plot of the wave function of the occupied surface state with the highest energy at the $M$ point of the BZ [see Fig. 7(f)] shows that this state is localized mainly at the Sn atom in the direction of the removed O atom. This indicates that the dangling bonds of the Sn ions, that are caused by the removal of the surface O atom, strongly contribute to the formation of the surface band. The energetic position of the Fermi level is above these surface states. Hence, the surface band states are occupied and the surface is also insulating. The dispersion of these bands is in accordance with GGA calculations by Batzill.[6]

### D. (111) surface

The band structure of the $(111)_{\mathrm{Sn}}$ surface is plotted along the path $\Gamma - X - Y' - Y - \Gamma$ across the BZ of the oblique Bravais lattice.[52] This surface exhibits three surface bands in the fundamental bulk band gap [cf. Fig. 8(a)] that are all valence bands. The main contributions to the formation of these bands arise from the Sn ions of the topmost layer ($s$ states) and the O ions of the second atomic layer ($p$ states) and, hence occupied dangling bonds form the surface bands. This can, again, be explained by a charge transfer from Sn dangling bonds into O 2$p$ orbitals as explained before. This picture is confirmed by the plot of the wave function in Fig. 8(b) and similar surface states have been reported by Duan.[18]

### E. Ionization energies and electron affinities

The ionization energy $I$ and electron affinity $A$ are calculated as differences between the band edges of the bulk electronic structure and the vacuum level from the slab

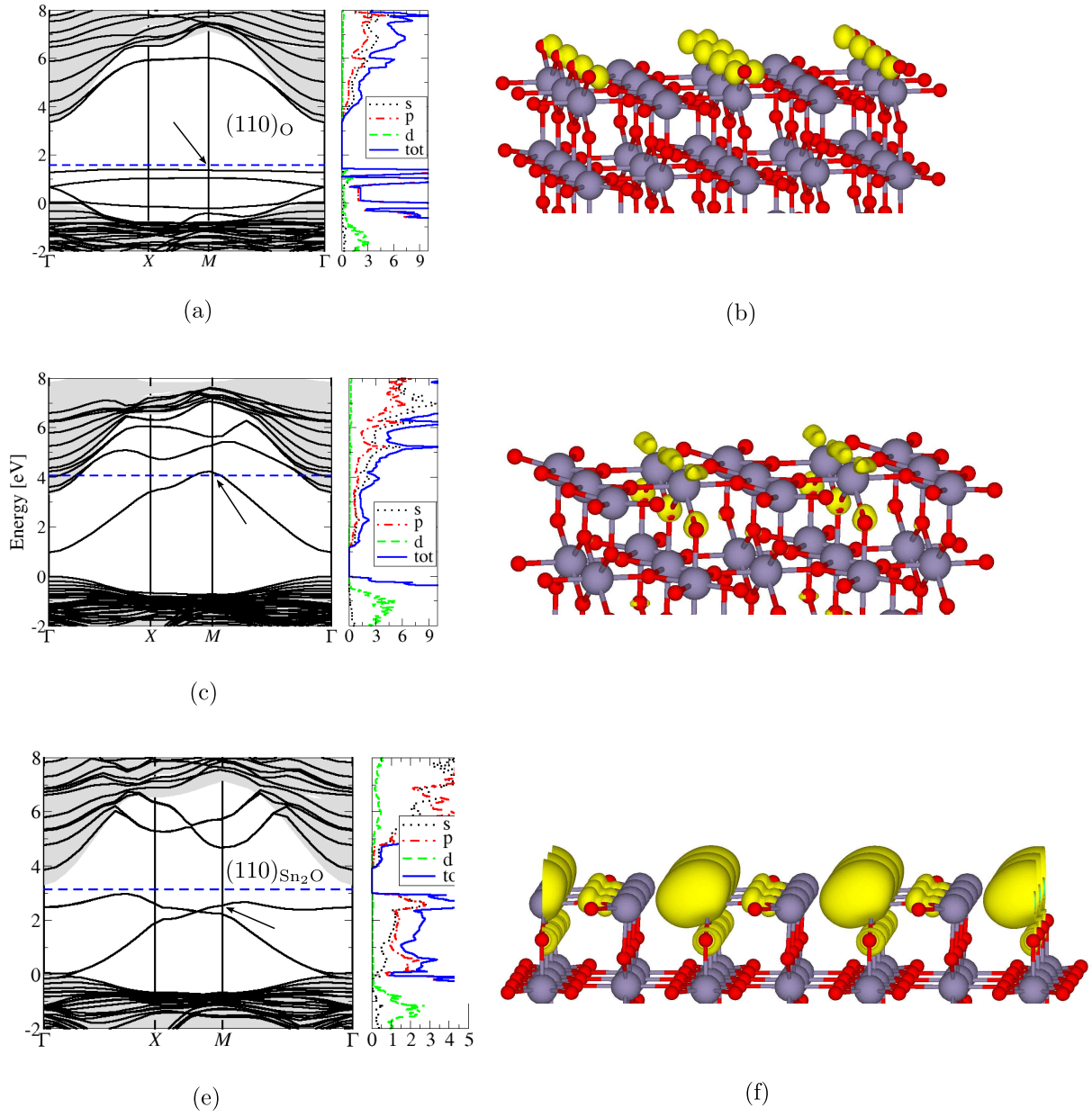


FIG. 7. (Color online) The band structure and DOS of the $(110)_{\mathrm{O}}$ surface (a), the $(110)_{\mathrm{SnO}}$ surface (b), or the $(110)_{\mathrm{Sn_2O}}$ surface (c), calculated using the LDA-$\frac{1}{2}$ scheme, is compared to the projected bulk bands (shaded area), respectively. The wave-functions of the highest occupied surface band states at $X$ (b) or the pronounced surface band at $M$ [(d) and (f)] are plotted as yellow isosurfaces of the same probabilities [the corresponding states are marked by the arrows].

calculation.[76] The alignment of the energy scales of the two calculations is done by the electrostatic potential, averaged over the plane parallel to the surface and plotted in perpendicular direction (see, for instance, Ref. 30 for details). The band edges of the bulk band structure are taken from HSE+$G_0W_0$ calculations.[17]

The resulting ionization energies and electron affinities as well as their dependence on the surface orientation and termination are summarized in Table IV. We want to emphasize, that the relaxation of the surface atoms significantly influences the results. For instance, in the case of the $(001)_{\mathrm{SnO_2}}$ surface the barrier $I$ for the electrons is increased by 0.8 eV compared to the unrelaxed surface. The reason for this large increase is the relative shift of the Sn and O ions at the surface that creates a surface dipole.

In addition, it is remarkable that for the O terminated (100) surface, the values for $I$ and $A$ are by up to $\approx$ 2.1 eV larger than those for the Sn terminated one. This is caused by the

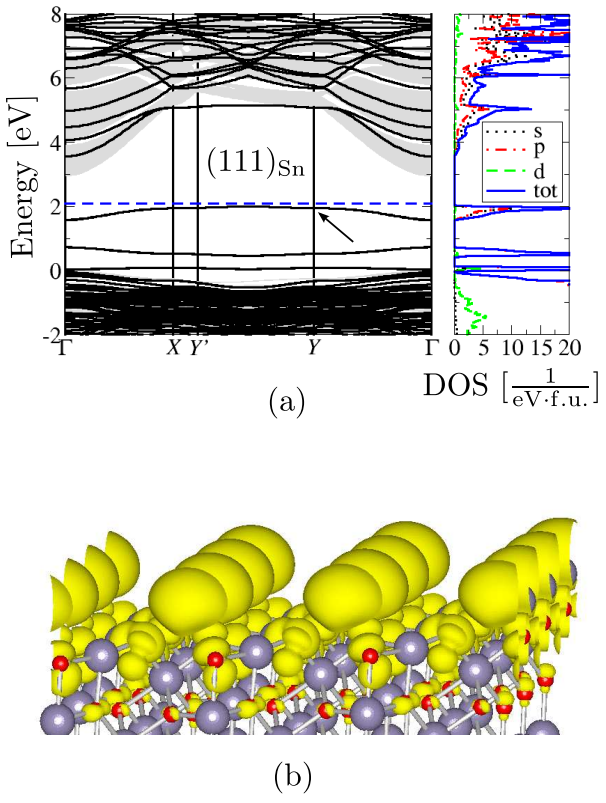


FIG. 8. (Color online) In (a) the band structure and DOS of the $(111)_{Sn}$ surface, calculated using the LDA-$\frac{1}{2}$ scheme, is compared to the projected bulk bands (shaded area), respectively. In (b) the square of the wave-function of the uppermost valence band at $Y$ is plotted as isosurfaces representing the same probabilities [the corresponding state is marked by the arrow in (a)].

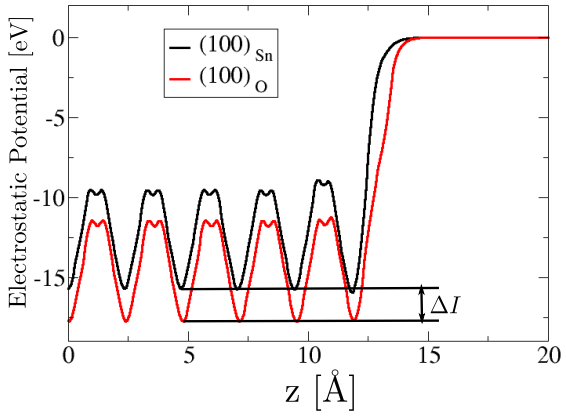


FIG. 9. (Color online) The perpendicular to the $z$-direction plane-averaged electrostatic potentials for the two terminations of the (100) surface. The Plots are aligned with respect to the vacuum level, the difference in the surface barriers between the oxygen- and the tin termination is indicated.

TABLE IV. Ionization energies $I$ (in eV) and electron affinities $A$ (in eV) of the surfaces investigated in this work. Values from Ref. 30, calculated for unrelaxed surfaces, are given for comparison.

| Surface | $I$ (eV) | | $A$ (eV) | |
|---|---|---|---|---|
| | This work | Ref. 30 | This work | Ref. 30 |
| $(001)_{SnO_2}$ | 8.08 | 7.08 | 4.45 | 3.45 |
| $(100)_O$ | 9.62 | | 5.99 | |
| $(100)_{Sn}$ | 7.57 | 7.73 | 3.94 | 4.10 |
| $(110)_O$ | 7.65 | | 4.02 | |
| $(110)_{SnO}$ | 7.30 | | 3.67 | |
| $(110)_{Sn_2O}$ | 8.07 | | 4.40 | |
| $(111)_{Sn}$ | 7.72 | | 4.09 | |

larger surface dipole in case of oxygen termination. In Fig. 9 the electrostatic potential averaged over planes perpendicular to the $z$ direction is shown for both terminations of the (100) surface. It becomes clear how the different surface barriers emerge from the different energetic distances between the bulk-like states (minima of the potential) and the vacuum level. The influence of the termination is much smaller for the (110) surface (cf. Table IV) due to the lower polarity of the (110) face. There is no complete cationic Sn layer but a SnO layer with lower polarity, which decreases the surface dipole compared to the (100) surface which has well separated Sn and O layers.

The results in Table IV cover a wide range of $I$ and $A$ values characterizing the different surface barriers with an overall variation of 2.32 eV induced by different surface orientations and terminations. Previously computed values for unrelaxed $SnO_2$ surfaces[30] show that there is an increase of 1 eV of the surface barriers of the $(001)_{SnO_2}$ surface, which is similar to our finding of 0.8 eV. In the case of the $(100)_O$ surface, the values for the unrelaxed atomic geometries are 0.16 eV higher[30] than those that we computed. This might be caused by the outward relaxation of the topmost atomic layers which decreases the surface dipole. Except for the values calculated from flat-band measurements on $SnO_2$ electrolyte interfaces[77] (without information on orientation or termination) there is no experimental data for comparison.

## VI. SUMMARY AND CONCLUSIONS

In this work we used density functional theory within the local density approximation to calculate the total energies and relaxed atomic geometries of unreconstructed low-index surfaces of $SnO_2$ with different orientations and terminations. We found that substantial atomic relaxations tend to passivate surface dangling bonds due to the formation of lone pairs in oxygen-derived states, in order to form the stable ionicities $Sn^{4+}$ and $Sn^{2+}$ in the surface layers. Atoms in the first layer tend to move outward from the surface. Only in the case of the O-terminated (110) surface the second $(SnO)_2$ layer is displaced stronger, leading to a separate layer with the uppermost oxygen atoms. We found the oxygen-terminated stoichiometric $(100)_O$ and $(110)_O$ surfaces to be the most stable ones in a

wide range of preparation conditions. Only under an extreme oxygen deficit the $(100)_{Sn}$ surface or the $(110)_{Sn_2O}$ surface become energetically more favorable.

In addition, we use the LDA-$\frac{1}{2}$ scheme to approximately simulate the QP excitation effects for the calculation of the electronic structure of the different surfaces. The tendency for complete filling or emptying of the surface states leads to insulating surfaces with surface gaps. Only for the $(110)_{SnO}$ surface the situation is not completely clear due to strong surface band dispersion. More detailed studies with a more sophisticated treatment of the QP effects are needed to clarify this point.

The different surface orientations, terminations, atomic geometries, and electronic structures modify the macroscopic surface dipole. As a consequence, the surface barriers for electron emission and escape vary significantly with the surface orientation and termination. We calculated variations of the ionization energy and electron affinity of about 2.3 eV between the $(110)_{SnO}$ and $(100)_{O}$ surfaces.

## ACKNOWLEDGMENTS

We thank J. Furthmüller and J. B. Varley for helpful and interesting scientific discussions. Support from the German Federal Government (BMBF Project No. 13N9669) and the Austrian Fond zur Förderung der Wissenschaftlichen Forschung in the framework of SFB25 Infrared Optical Nanostructures is gratefully acknowledged. Part of this work was performed under the auspices of the U.S. Department of Energy at Lawrence Livermore National Laboratory under Contract DE-AC52-07A27344.

* sebastian.kuefner@uni-jena.de


1 D. S. Ginley and C. Bright, MRS Bull. **25**, 15 (2000).
2 E. Fortunato, D. Ginley, H. Hosono, and D. C. Paine, MRS Bull. **32**, 242 (2007).
3 J. Haines and J. M. Léger, Phys. Rev. B **55**, 11144 (1997).
4 A. A. Bolzan, C. Fong, B. J. Kennedy, and C. J. Howard, Acta Crystallogr. B **53**, 373 (1997).
5 A. Klein, C. Körber, A. Wachau, F. Säuberlich, Y. Gassenbauer, S. P. Harvey, D. E. Proffit, and T. O. Mason, Materials **3**, 4892 (2010).
6 M. Batzill and U. Diebold, Prog. Surf. Sci. **79**, 47 (2005).
7 M. Batzill, Sensors **6**, 1345 (2006).
8 Z. Q. Li, Y. L. Yin, X. D. Liu, L. Y. Li, H. Liu, and Q. G. Song, J. Appl. Phys. **106**, 083701 (2009).
9 P. A. Cox, R. G. Egdell, C. Harding, A. F. Orchard, W. R. Patterson, and P. J. Tavener, Solid State Commun. **44**, 837 (1982).
10 P. Cox, R. Egdell, C. Harding, W. Patterson, and P. Tavener, Surf. Sci. **123**, 179 (1982).
11 M. E. White, O. Bierwagen, M. Y. Tsai, and J. S. Speck, J. Appl. Phys. **106**, 093704 (2009).
12 Ç. Kılıç and A. Zunger, Phys. Rev. Lett. **88**, 095501 (2002).
13 J. Robertson, Rep. Prog. Phys. **69**, 327 (2006).
14 H. Peelaers, E. Kioupakis, and C. G. Van de Walle, Appl. Phys. Lett. **100**, 011914 (2012).
15 S. Lany and A. Zunger, Phys. Rev. Lett. **98**, 045501 (2007).
16 K. Reimann and M. Steube, Solid State Commun. **105**, 649 (1998).
17 A. Schleife, J. B. Varley, F. Fuchs, C. Rödl, F. Bechstedt, P. Rinke, A. Janotti, and C. G. Van de Walle, Phys. Rev. B **83**, 035116 (2011).
18 Y. Duan, Phys. Rev. B **77**, 045332 (2008).
19 A. Seko, A. Togo, F. Oba, and I. Tanaka, Phys. Rev. Lett. **100**, 045702 (2008).
20 D. F. Cox, T. B. Fryberger, and S. Semancik, Phys. Rev. B **38**, 2072 (1988).
21 M. Batzill, K. Katsiev, J. M. Burst, U. Diebold, A. M. Chaka, and B. Delley, Phys. Rev. B **72**, 165414 (2005).
22 C. Körber, P. Ágoston, and A. Klein, Sensors Actuat. B Chem. **139**, 665 (2009).
23 J. M. Themlin, R. Sporken, J. Darville, R. Caudano, J. M. Gilles, and R. L. Johnson, Phys. Rev. B **42**, 11914 (1990).
24 C. L. Pang, S. A. Haycock, H. Raza, P. J. Möller, and G. Thornton, Phys. Rev. B **62**, R7775 (2000).
25 A. Beltran, J. Andres, E. Longo, and E. R. Leite, Appl. Phys. Lett. **83**, 635 (2003).
26 T. T. Rantala, T. S. Rantala, and V. Lantto, Surf. Sci. **420**, 103 (1999).
27 T. T. Rantala, T. S. Rantala, and V. Lantto, Mat. Sci. Semicon. Proc. **3**, 103 (2000).
28 M. A. Mäki-Jaskari and T. T. Rantala, Phys. Rev. B **64**, 075407 (2001).
29 P. Ágoston and K. Albe, Surf. Sci. **605**, 714 (2011).
30 B. Höffling, A. Schleife, F. Fuchs, C. Rödl, and F. Bechstedt, Phys. Rev. B **85**, 035305 (2012).
31 L. G. Ferreira, M. Marques, and L. K. Teles, Phys. Rev. B **78**, 125116 (2008).
32 P. Hohenberg and W. Kohn, Phys. Rev. **136**, B864 (1964).
33 W. Kohn and L. J. Sham, Phys. Rev. **140**, A1133 (1965).
34 D. M. Ceperley and B. J. Alder, Phys. Rev. Lett. **45**, 566 (1980).
35 J. P. Perdew and A. Zunger, Phys. Rev. B **23**, 5048 (1981).
36 G. Kresse and J. Furthmüller, Phys. Rev. B **54**, 11169 (1996).
37 G. Kresse and J. Furthmüller, Comp. Mat. Sci. **6**, 15 (1996).
38 P. E. Blöchl, Phys. Rev. B **50**, 17953 (1994).
39 G. Kresse and D. Joubert, Phys. Rev. B **59**, 1758 (1999).
40 H. J. Monkhorst and J. D. Pack, Phys. Rev. B **13**, 5188 (1976).
41 W. G. Aulbur, L. Jönsson, and J. W. Wilkins, in *Advances in Research and Applications*, Solid State Physics, Vol. 54, edited by H. Ehrenreich and F. Spaepen (Academic Press, 1999) pp. 1–218.
42 F. Fuchs, J. Furthmüller, F. Bechstedt, M. Shishkin, and G. Kresse, Phys. Rev. B **76**, 115109 (2007).
43 F. Bechstedt, F. Fuchs, and G. Kresse, Phys. Status Solidi B **246**, 1877 (2009).
44 A. Schleife, C. Rödl, F. Fuchs, J. Furthmüller, and F. Bechstedt, Phys. Rev. B **80**, 035112 (2009).
45 L. C. de Carvalho, A. Schleife, F. Fuchs, and F. Bechstedt, Appl. Phys. Lett. **97**, 232101 (2010).
46 L. C. de Carvalho, A. Schleife, and F. Bechstedt, Phys. Rev. B **84**, 195105 (2011).
47 J. Heyd, G. E. Scuseria, and M. Ernzerhof, J. Chem. Phys. **124**, 219906 (2006).
48 J. Paier, M. Marsman, K. Hummer, G. Kresse, I. C. Gerber, and J. G. Ángyán, J. Chem. Phys. **125**, 249901 (2006).
49 A. Belabbes, J. Furthmüller, and F. Bechstedt,

Phys. Rev. B **84**, 205304 (2011).
[50] J. R. Leite and L. G. Ferreira, Phys. Rev. A **3**, 1224 (1971).
[51] J. C. Slater and K. H. Johnson, Phys. Rev. B **5**, 844 (1972).
[52] F. Bechstedt, *Principles of Surface Physics* (Springer-Verlag, Berlin, 2003).
[53] J. Neugebauer and M. Scheffler, Phys. Rev. B **46**, 16067 (1992).
[54] P. W. Tasker, J. Phys. C Solid State **12**, 4977 (1979).
[55] J. Goniakowski, F. Finocchi, and C. Noguera, Rep. Prog. Phys. **71**, 016501 (2008).
[56] K. Reuter and M. Scheffler, Phys. Rev. B **65**, 035406 (2001).
[57] H. Landolt and R. Börnstein, *Zahlenwerte und Funktionen aus Physik, Chemie, Astronomie, Geophysik und Technik*, Vol. 6 (Springer-Verlag, Berlin, 1982).
[58] D. Hobbs, G. Kresse, and J. Hafner, Phys. Rev. B **62**, 11556 (2000).
[59] D. R. Lide, *CRC handbook of chemistry and physics: a ready-reference book of chemical and physical data*, CRC Handbook of Chemistry and Physics, 85th Ed (CRC Press, 2004).
[60] N. I. Medvedeva, V. P. Zhukov, M. Y. Khodos, and V. A. Gubanov, Phys. Status Solidi B **160**, 517 (1990).
[61] C. Kittel, *Introduction to Solid State Physics*, 8th ed. (John Wiley and Sons Inc., New York, Chichester, 2005).
[62] K. Ellmer, J. Phys. D Appl. Phys. **34**, 3097 (2001).
[63] G. McCarthy and J. Welton, Powder Diffr. **4**, 156 (1989).
[64] F. D. Murnaghan, P. Natl. Acad. Sci. USA **30**, 244 (1944).
[65] X. J. Kong, C. T. Chan, K. M. Ho, and Y. Y. Ye, Phys. Rev. B **42**, 9357 (1990).
[66] J. P. Perdew, J. A. Chevary, S. H. Vosko, K. A. Jackson, M. R. Pederson, D. J. Singh, and C. Fiolhais, Phys. Rev. B **46**, 6671 (1992).
[67] D. Fröhlich, R. Kenklies, and R. Helbig, Phys. Rev. Lett. **41**, 1750 (1978).
[68] R. Ramprasad, H. Zhu, P. Rinke, and M. Scheffler, Phys. Rev. Lett. **108**, 066404 (2012).
[69] E. de Frésart, J. Darville, and J. Gilles, Solid State Commun. **37**, 13 (1981).
[70] E. de Frésart, J. Darville, and J. Gilles, Appl. Surf. Sci. **11/12**, 637 (1982).
[71] S. Munnix and M. Schmeits, Phys. Rev. B **27**, 7624 (1983).
[72] W. Bergermayer and I. Tanaka, Appl. Phys. Lett. **84**, 909 (2004).
[73] P. A. Mulheran and J. H. Harding, Modelling Simul. Mater. Sci. Eng. **1**, 39 (1992).
[74] E. R. Leite, T. R. Giraldi, F. M. Pontes, E. Longo, A. Beltrán, and J. Andrés, Appl. Phys. Lett. **83**, 1566 (2003).
[75] J. Oviedo and M. Gillan, Surf. Sci. **463**, 93 (2000).
[76] R. L. Anderson, Solid State Electron. **5**, 341 (1962).
[77] M. A. Butler and D. S. Ginley, J. Electrochem. Soc. **125**, 228 (1978).